ELSEVIER

Polymer Degradation and Stability 76 (2002) 25–36

Polymer Degradation and Stability

www.elsevier.com/locate/polydegstab

Thermal degradation at 393 K of poly(acrylonitrile-butadiene-styrene) (ABS) containing a hindered amine stabilizer: a study by 1D and 2D electron spin resonance imaging (ESRI) and ATR–FTIR

Mikhail V. Motyakin, Shulamith Schlick*

Department of Chemistry, University of Detroit Mercy, Detroit, MI 48219, USA

Received 18 July 2001; received in revised form 30 October 2001; accepted 4 November 2001

Abstract

Electron spin resonance imaging (ESRI) was developed in our laboratory as a method for spatial and spectral profiling of radicals formed during polymer degradation. We present the application of this approach to the study of thermal degradation at 393 K of poly(acrylonitrile-butadiene-styrene) (ABS) containing 1 or 2% w/w Tinuvin 770 as the hindered amine stabilizer (HAS). The spatial distribution of the HAS-derived nitroxide radicals, obtained by 1D ESRI, was homogeneous at short treatment times but became heterogeneous after treatment times $\geqslant$ 70 h. The spatial variation of the ESR line shapes with sample depth was visualized by 2D spectral–spatial ESRI. Nondestructive (''virtual'') slicing of the 2D images resulted in a series of ESR spectra along the sample depth, which were used to deduce the relative intensity of nitroxide radicals present in two distinct sites. The two sites represent radicals located in butadiene-rich and SAN-rich domains, respectively. Taken together, 1D and 2D ESRI allowed the determination of the extent of degradation within morphologically-distinct domains as a function of sample depth and treatment time. The conclusions from the ESRI experiments were substantiated by attenuated total reflectance (ATR) FTIR spectroscopy of the outer layer (500 μm thick) of the polymer. Comparison of the two techniques suggested that the advantage of the ESRI method is its ability to provide mechanistic details on the *early* stages of the ageing process. ESRI and FTIR data indicated that the larger Tinuvin 770 content in the polymer, 2%, leads to less efficient stabilization.

Keywords: Polymer degradation; Hindered amine stabilizers (HAS); Electron spin resonance (ESR); Electron spin resonance imaging (ESRI)

1. Introduction and background

Degradation profiles provide essential information for predicting the behaviour and lifetime of polymeric materials exposed to UV and high-energy irradiation, or to thermal and mechanical stresses. The extent of degradation and its spatial variation depend on the formation of unstable intermediates, and on the transport of atmospheric oxygen through the sample. When the consumption of oxygen in degradation processes is comparable or lower than the amount of oxygen provided by diffusion from the atmosphere, degradation can occur through the entire sample thickness. If, however, the rate of oxygen consumption is higher than its supply rate, as is often the case in accelerated ageing in the laboratory, only thin surface layers in contact with air are degraded, while the sample interior is little, if at all, affected; this is the diffusion-limited oxidation (DLO) regime [1,2]. The delicate balance between oxygen supply and consumption can be further complicated by changes in the diffusion rate of oxygen due to changes in the polymer upon degradation, for instance chain scission or cross-linking.

The DLO concept also implies that lifetimes of polymeric materials deduced from the study of *average* properties for samples involved in accelerated degradation cannot be used to estimate the durability of polymers in normal exposures and use. For this reason methods for measuring the spatial distribution of polymer properties due to degradation have been developed. Density profiling [3] and modulus profiling [4–6], for instance, are excellent methods, especially at advanced stages in the degradation process. Both profiling methods are destructive, in the sense that the sample is cut into sections and each section is studied separately.

* Corresponding author. Tel.: +1-313-993-1012; fax: +1-313-993-1144.

E-mail address: schlicks@udmercy.edu (S. Schlick).

0141-3910/02/$ - see front matter
PII: S0141-3910(01)00262-2

Recently IR microscopy [7,8] and chemiluminescence methods [9–11] have been used to extract important mechanistic details.

Our group has developed 1D and 2D electron spin resonance imaging (ESRI) methods in order to deduce the spatial variation of radicals formed during polymer degradation and stabilization. Imaging is based on encoding spatial information in the ESR spectra via magnetic field gradients [12–15]. By 1D ESRI it is possible to deduce the distribution of radicals along the gradient direction [15,16]. 2D spectral–spatial ESRI can be used in order to follow *nondestructively* the spatial variation of the line shapes and relative intensities of the various spectral components along the same direction [12–14,17,18].

In previous papers we have described the application of this approach to the study of photodegradation of poly(acrylonitrile-butadiene-styrene) (ABS) containing Tinuvin 770 as the hindered amine stabilizer (HAS) [16–18]. The repeat units in ABS and the amine are shown in Fig. 1. In these studies the direction of the magnetic field gradient was along the sample depth. Important details on the degradation process were based on the detection of two sites for the HAS-derived nitroxides, which were assigned to radicals located in domains differing in their monomer composition. The spatial distribution of the radical intensity obtained by 1D ESRI was heterogeneous as a result of irradiation using Xe or UVB ($\lambda = 290$–320 nm) sources; by contrast, the distribution of nitroxides produced during thermal degradation at 333 K was approximately spatially homogeneous after $\approx$800 h of treatment [17,18].

The stabilizing effect of hindered amines in photodegradation is widely documented; the amines are, however, considered less effective as thermal stabilizers [19]. In accelerated degradation polymers are exposed not only to UV radiation but also to high temperatures. For this reason we have initiated a study by 1D and 2D spectral–spatial ESRI of the thermal degradation at elevated temperatures, 393 K, in ABS samples containing 1 or 2% w/w Tinuvin 770. The main objective of this study was to investigate the specific effect of hindered amine light stabilizers on the rate of thermal ageing. As will be seen below, the imaging results indicated that the degradation is spatially-heterogeneous for thermal treatment at 393 K, and that the larger Tinuvin 770 content (2%) in the polymer leads to less efficient stabilization. The conclusions deduced from the ESRI experiments were confirmed by attenuated total reflectance (ATR) IR measurements. Some results have been reported [20].

1D ESRI has been used to deduce the intensity profiles of nitroxides during photodegradation of polypropylene containing HAS [21,22]. For a heterophasic system such as ABS, it is important to determine the evolution of the nitroxides in each morphological domain; for this reason the intensity profiles determined by 1D ESRI were complemented by the spatial variation of the ESR spectra deduced from 2D spectral–spatial ESRI [16–18].

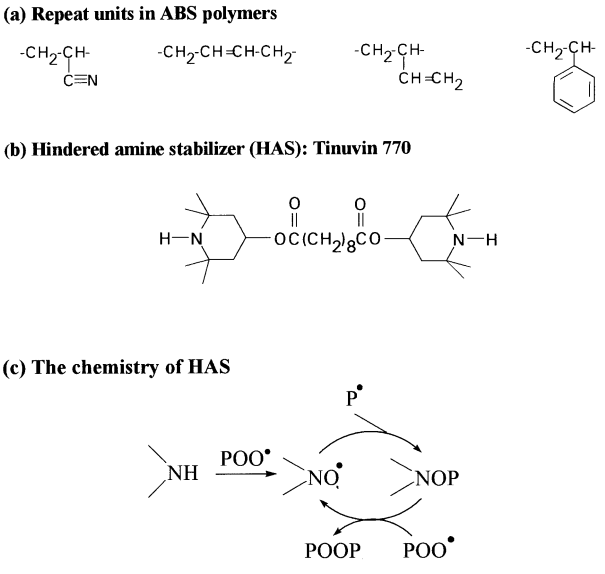

Fig. 1. Repeat units in ABS, and Tinuvin 770.

2. Experimental

2.1. Sample preparation

Thermal degradation experiments were performed by heat treatment of poly(acrylonitrile-butadiene-styrene (ABS Magnum 342 EZ, from Dow Chemical Company) doped with 1 or 2% w/w of (bis(2,2,6,6-tetramethyl-4-piperidinyl) sebacate), the hindered amine stabilizer (HAS) known as Tinuvin 770 from Ciba Specialty Chemicals (Fig. 1). The polymer and the HAS were blended, shredded, and shaped into $10\times10\times0.4$ cm plaques in an injection molding machine at 483 K. The plaques were thermally treated in a convection oven at 393 K. For the ESR imaging experiments, cylindrical samples 4 mm in diameter were cut from the plaques, and the samples were placed in the ESR resonator with the symmetry axis along the field gradient. Additional details have been reported [16–18].

The notation used for describing the results are ABS0H, ABS1H, and ABS2H for polymer samples containing, respectively, 0, 1 and 2% HAS.

2.2. ESR imaging and data acquisition

In the presence of a gradient, the ESR signal is a convolution of the ESR spectrum in the absence of the gradient with the distribution of the paramagnetic centers along the gradient direction [23]; this is the 1D image. These images were obtained with field gradients of 125 G/cm (for treatment times of 24 and 72 h) and

200 G/cm (for all other samples). The ESR spectra and 1D images were measured at 240 K to avoid the spatial dependence of the ESR signal [16]. The concentration profiles were obtained by simulation of the 1D image followed by deconvolution.

In previous studies we have deduced the concentration profiles by Fourier transform followed by optimization with the Monte-Carlo procedure. The disadvantage of this method is the high frequency noise that is introduced when sharp edges in the profile are desirable. In order to remove the noise, the intensity profile was fitted by an analytical function and convoluted with the ESR spectrum measured in the absence of magnetic field gradient. The "best fit" was obtained by slight variations of the parameters of the chosen analytical function in order to get good agreement with the 1D image [24].

The 2D spectral–spatial ESRI images were reconstructed from a complete set of projections (typically 128) collected as a function of the magnetic field gradient, using a convoluted back-projection algorithm [12–14]. In the initial step the projections at the missing angles were assumed to be identical with the projection measured at the largest available angle. The projections at the missing angles were then obtained by the projection slice algorithm (PSA) [25,26] with two iterations. The 2D images are displayed on a 128×128 grid.

2.3. ATR–FTIR measurements

ATR–FTIR spectra were measured with the Perkin-Elmer FTIR Spectrum 2000 spectrometer equipped with a horizontal attenuated total reflectance (HATR) accessory. Sections of thickness 500 μm were cut from the samples and dissolved in methylene chloride (from Fisher Scientific Company). The polymer solution was poured directly on the ZnSe ATR crystal and a polymer film was obtained by solvent evaporation. The measurements were carried out in the range 700–4000 cm^{-1}, with 8 scans and resolution of 4 cm^{-1}. The spectra were then corrected for ATR, baseline corrected and normalized to the 2238 cm^{-1} peak height (acrylonitrile peak), which was assumed to be invariant during thermal treatment [27].

3. Results

3.1. Concentration and ESR spectra of HAS-derived nitroxides

The ESR spectra at 300 K of the HAS-derived nitroxide in heat-treated ABS consist of a superposition of two components, from nitroxide radicals differing in their mobility: a "fast" component (F, extreme width ≈32 G), and a "slow" component (S, extreme width ≈64 G). A typical ESR spectrum at 300 K is shown in the inset of Fig. 2, for ABS2H after 241 h of thermal treatment at 393 K. The rotation of the nitroxides is determined by two factors: the free volume in the polymer, and the dynamical fluctuations due to the segmental motion of the polymer chains. For these reasons, we assign the F and S components to nitroxides located respectively in low-T_g domains rich in linear polybutadiene (PB), and in high-T_g domains rich in poly(styrene-*co*-acrylonitrile) (SAN) or in cross-linked PB [16–18]. The presence of the two spectral components, F and S, is due to the heterophasic nature of ABS [7,28,29]. As a result of polymer degradation, however, the F/S ratio varies with treatment time; this variation provides the connection to the degradation and stabilization processes. The determination of the F/S ratio has been described [16a].

The variation of %F and of the total nitroxide concentration in whole samples as a function of treatment time, t, is shown in Fig. 2. The relative intensity of the F component, Fig. 2A, first increases, then decreases with

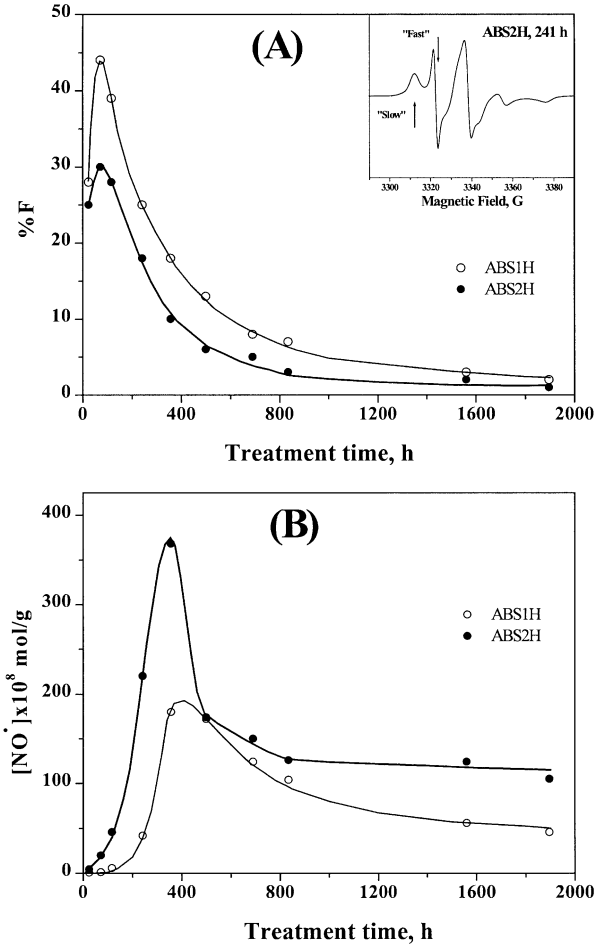

Fig. 2. Relative concentration of the fast component, %F in (A), and total nitroxide concentration in mol/g of sample in (B), for ABS1H and ABS2H as a function of treatment time at 393 K. The solid lines in (A) and (B) were drawn by nonlinear regression. The inset in (A) is the ESR spectrum at 300 K of ABS2H after 241 h of thermal treatment at 393 K.

increasing thermal treatment time, and becomes negligible ($\leqslant 3\%$ of the total intensity) for $t = 1896$ h. As in photodegradation, we interpret the decrease of %F with treatment time as due to the consumption of the HAS-derived nitroxide radicals located in the butadiene-rich domains of the polymer, because PB is more vulnerable to degradation compared to the other repeat units in ABS [30]. This interpretation is supported by the ATR–IR results, vide infra Figs. 8–10. The degradation processes in PB can lead to the consumption of the nitroxides; cross-linking is also possible, and the result is slower rotational motion of the nitroxides.

The total intensity of HAS-derived nitroxides, Fig. 2B, increases to a maximum for treatment time of ≈400 h for both ABS1H and ABS2H. Similar maxima in the nitroxide concentration have been detected in UV-exposed polymeric coatings containing 0.25–2% w/w HAS [31], and in ABS2H irradiated by a Xe source [18].

3.2. Concentration profiles of nitroxide deduced by 1D ESRI

In Figs. 3 and 4 we present the concentration profiles of nitroxides along the sample depth for ABS1H and ABS2H, respectively, for the indicated treatment times; the profiles were deduced by simulation of 1D ESR images measured at 240 K. All profiles on the right side are presented with the same maximum height; the profiles on the left are given for one side of the samples (because of symmetry), and normalized by the nitroxide concentration measured in whole samples, using data shown in Fig. 2B. The ABS1H profiles for treatment times of 24 and 72 h are not given in Fig. 3 because the corresponding nitroxide signals were weak. The evolution from flat profiles in the initial stages of thermal ageing to spatially heterogeneous profiles due to DLO is clearly seen in Figs. 3 and 4. The 1D profiles indicate that the HAS-derived nitroxides are located at the two sample extremities, in regions whose widths are 700–800 μm in ABS1H and 500–600 μm in ABS2H.

By combining the 1D profiles with the measurements of the nitroxide concentration in whole samples, it was possible to determine the %HAS that is present as nitroxide, as a function of sample depth for various treatment times. After 356 h the maximum %HAS present as nitroxide is ≈17% for ABS1H and ≈23% for ABS2H; these values were measured of course at the two extremities of the sample.

3.3. 2D spectral–spatial ESRI of HAS-derived nitroxides

In order to examine the spatial variation of the two spectral components, we performed 2D ESRI experiments on the thermally aged ABS containing HAS. The 2D spectral–spatial perspective and contour plots of

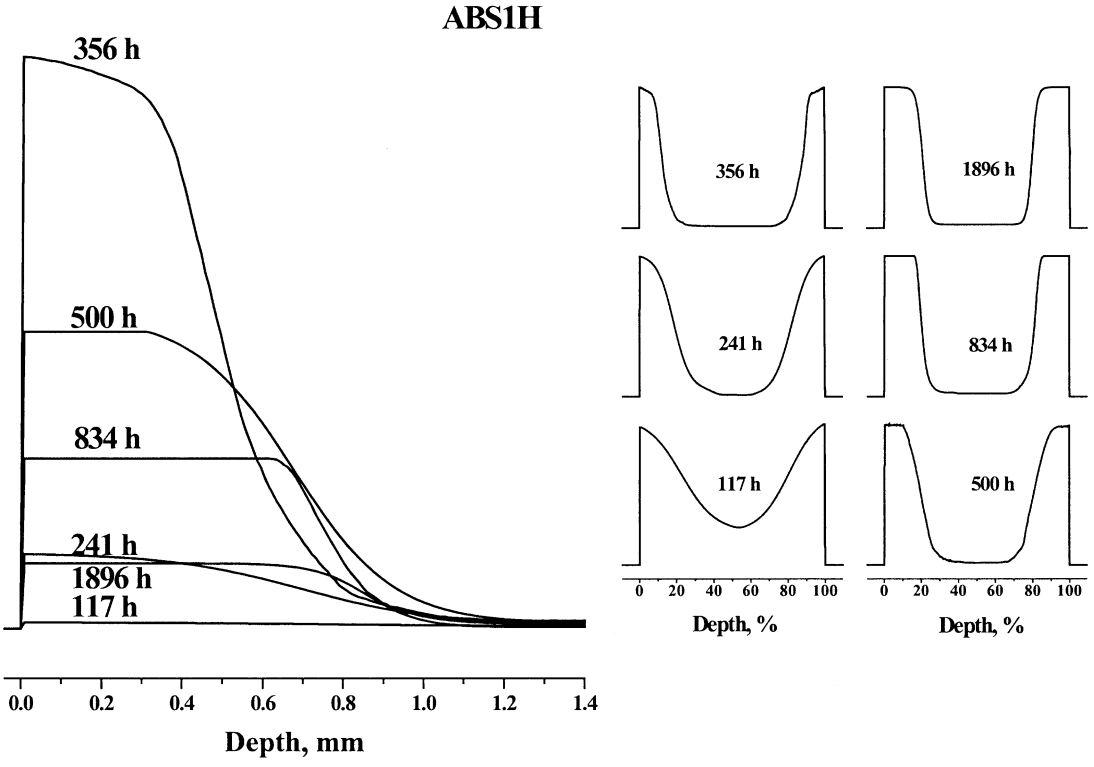

Fig. 3. Repeat units in ABS, Tinuvin 770 and the chemistry of HAS. Right: 1D concentration profiles of ABS1H for the indicated treatment times. Left: 1D concentration profiles normalized to the corresponding nitroxide concentration (shown in Fig. 2A). Only one side of each (symmetrical) profile is shown.

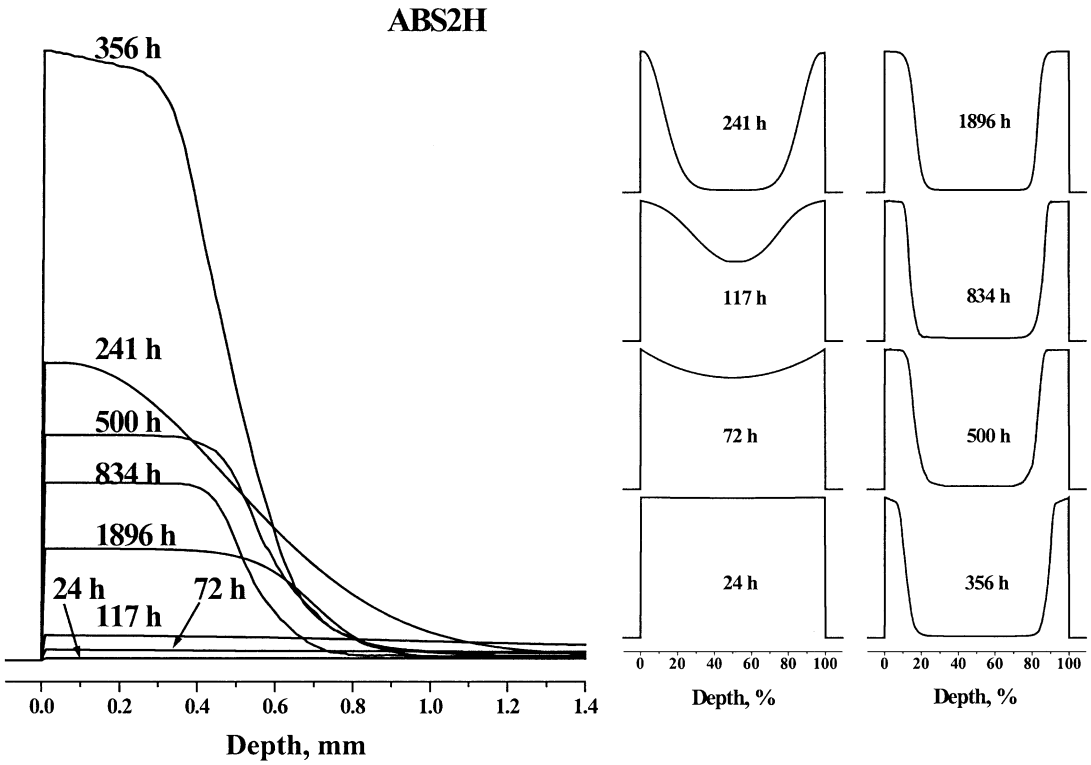

Fig. 4. Right: 1D concentration profiles for ABS2H for the indicated treatment times. Left: 1D concentration profiles normalized to the corresponding nitroxide concentration (shown in Fig. 2B). Only one side of each (symmetrical) profile is shown.

nitroxide radicals for treatment times of 241 and 834 h are given in Fig. 5 for ABS1H, and in Fig. 6 for ABS2H. The ESR intensity is presented in absorption. The contour and perspective plots show very clearly the distribution of the signal intensity, and the negligible signal intensity in the sample interior, as also seen in the concentration profiles deduced from 1D ESRI (Figs. 3 and 4).

The 2D images can be "sliced" *nondestructively* to give ESR spectra at various depths of the sample. These spectral slices indicate the spatial line shape variation and the relative intensity of each spectral component (F and S) as a function of sample depth. For the short treatment time ($t = 241$ h), the ESR spectra of the outer layers (thickness 200 μm) in contact with oxygen consist

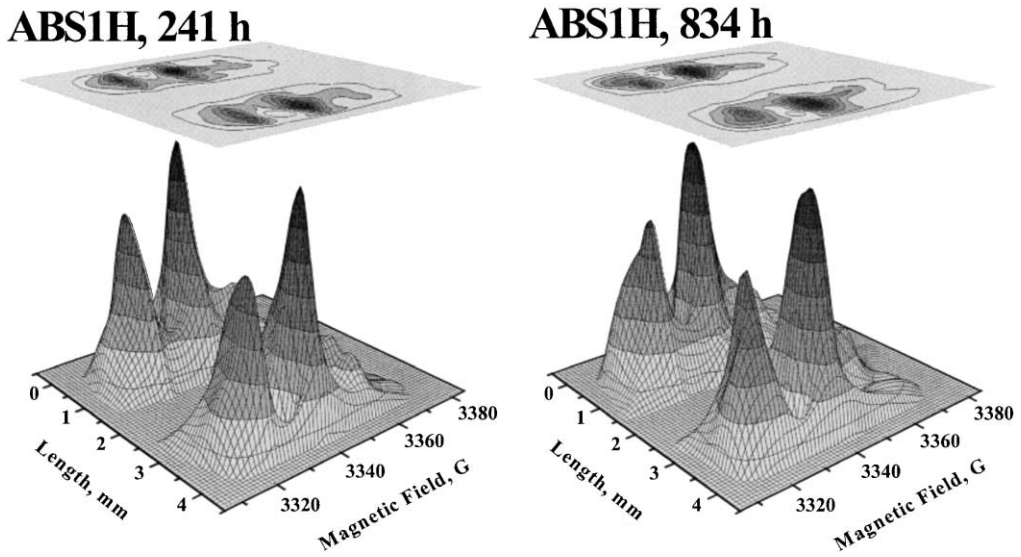

Fig. 5. 2D spectral–spatial contour and perspective plots of HAS-derived nitroxides in ABS1H after 241 h (left) and 834 h (right) of thermal treatment at 393 K, presented in absorption.

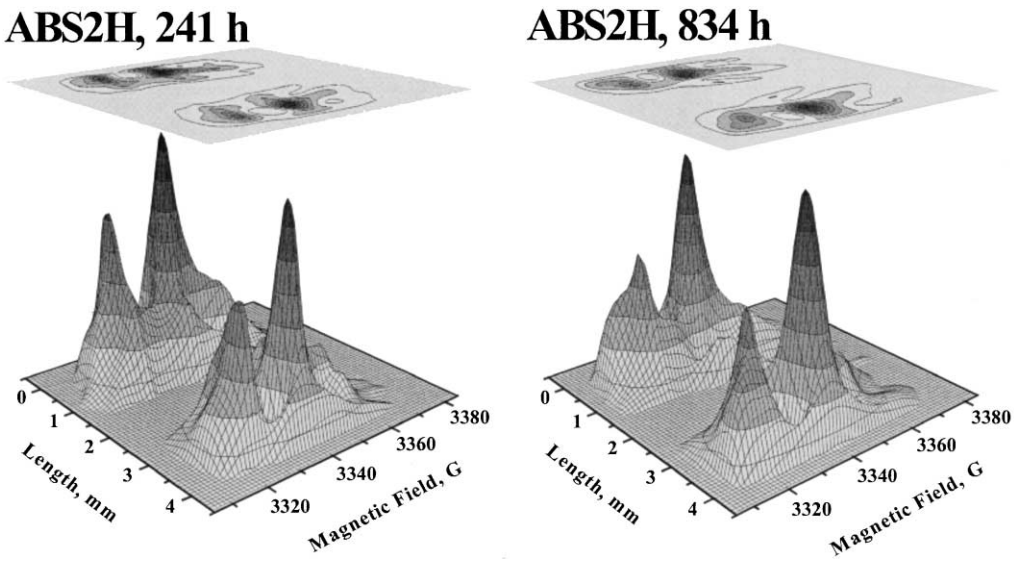

Fig. 6. 2D spectral–spatial contour and perspective plots of HAS-derived nitroxides in ABS2H after 241 h (left) and 834 h (right) of thermal treatment at 393 K, presented in absorption.

of two spectral components with %F≈21–24%. After 834 h of treatment the outer layers contain a negligible amount of the fast component, 3–5%, pointing to degradation of low-T_g butadiene-rich domains.

In Fig. 7 we show the results of *spectral profiling*: the evolution of the relative amount of the fast component within the sample depth for ABS1H ($t=241$ and 834 h) and ABS2H ($t=72$, 241 and 834 h). Corresponding %F profiles have been calculated for each treatment time. Since the F component was assigned to nitroxides located in PB (elastomeric) domains, spectral profiling emphasizes the changes that have occurred in these domains, and can thus be also termed *elastomer phase profiling*. The line shape profiles clearly indicate the progressive disappearance of the fast component with treatment time. Moreover, comparison of the profiles for ABS1H and ABS2H shows the presence of the fast component in a narrower part of the sample in ABS2H compared to ABS1H: in ABS2H the half maximum intensity of the fast component is at ≈500 μm for treatment time of 834 h, compared to ≈650 μm for ABS1H. In addition, for treatment times shorter than 834 h the minimum amount of %F is larger for ABS1H. After 241 h of thermal treatment the minimum %F is 13% in ABS2H and 18% in ABS1H; these numbers suggest that the loss of elastomeric properties is greater in ABS2H than in ABS1H.

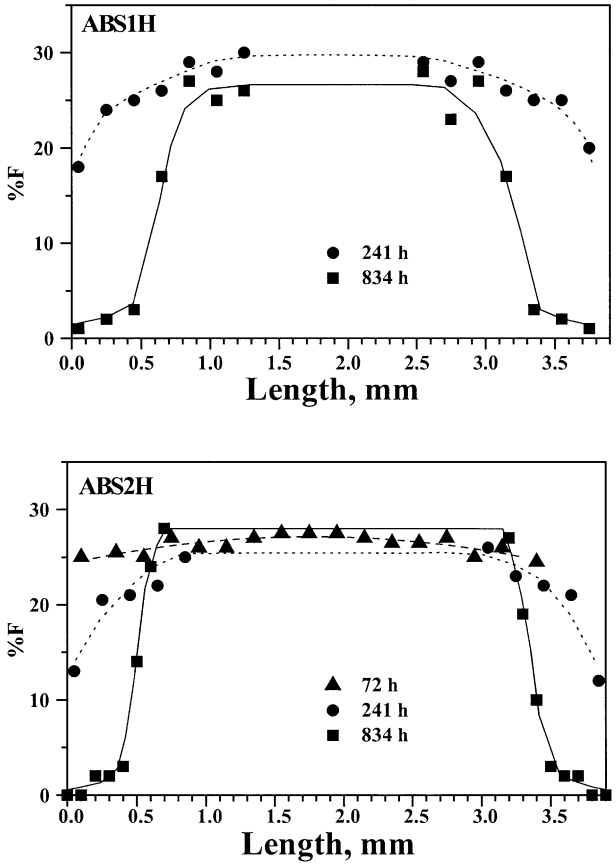

Fig. 7. Spectral profiling: %F as a function of sample depth for ABS1H (top) and ABS2H (bottom) for the indicated treatment times at 393 K. The data were deduced from 200 μm thick virtual (non-destructive) slices in the corresponding 2D ESR images.

3.4. ATR–FTIR measurements

The ATR–FTIR results are presented in Figs. 8–10. Fig. 8A shows spectra of the outer layer of thickness 500 μm for ABS0H (0), ABS1H (1), and ABS2H (2) after 1896 h of treatment at 393 K. The spectra clearly indicate that the concentration of degradation products in the hydroxyl (3300–3600 cm^{-1}) and carbonyl (1650–1800 cm^{-1}) regions is highest in ABS2H and lowest in ABS0H. For the same treatment time, the butadiene peak intensity at 966 cm^{-1} decreases in the same order.

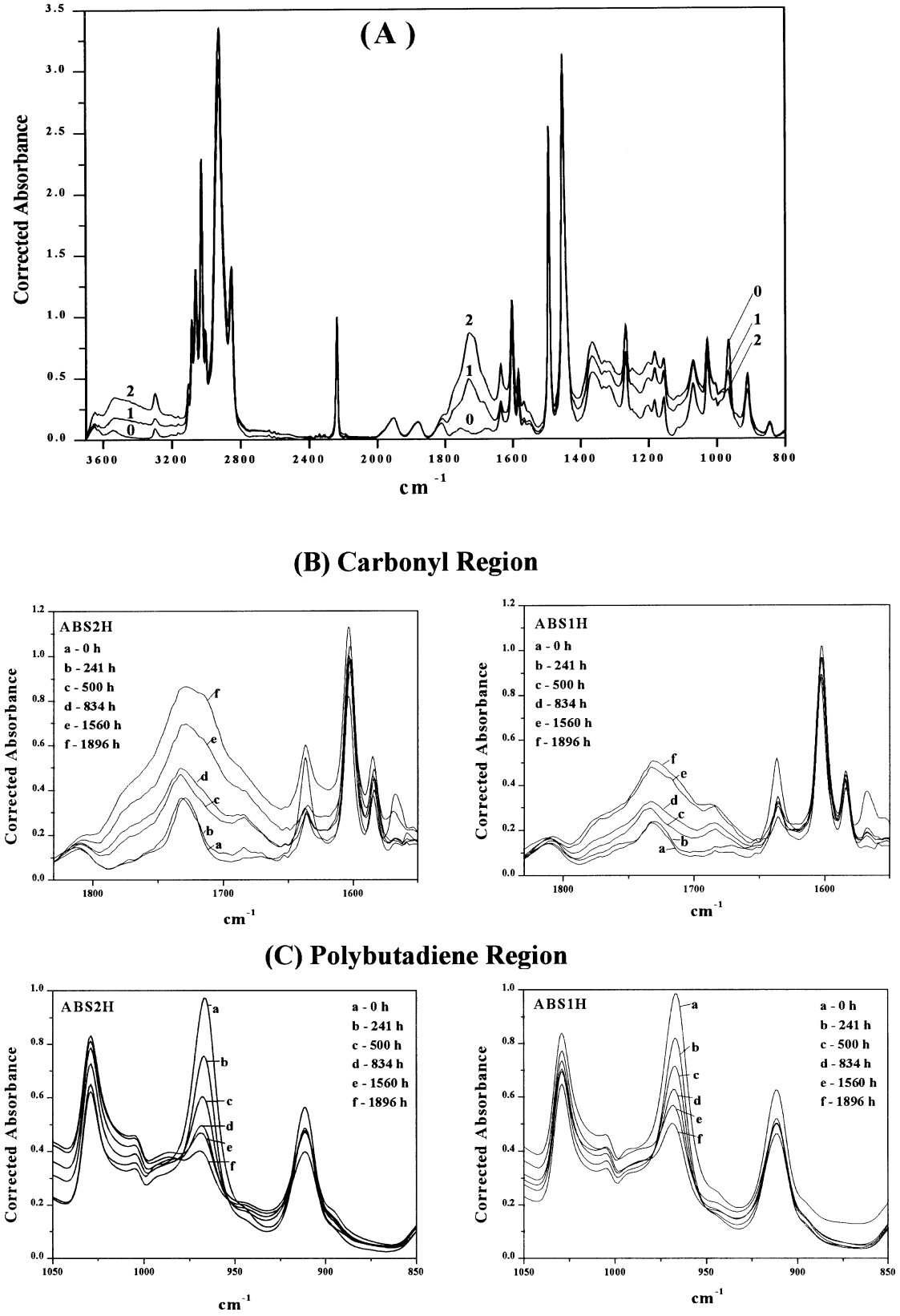

Fig. 8. (A) ATR–FTIR spectra of ABS0H (0), ABS1H (1) and ABS2H (2) treated for 1896 h at 393 K. (B) Changes in the carbonyl region for ABS2H and ABS1H with treatment time: a, 0 h; b, 241 h; c, 500 h; d, 834 h; e, 1560; h; f, 1896 h. (C) Changes in the butadiene region for ABS2H and ABS1H with treatment time: a, 0 h; b, 241 h; c, 500 h; d, 834 h; e, 1560 h; f, 1896 h.

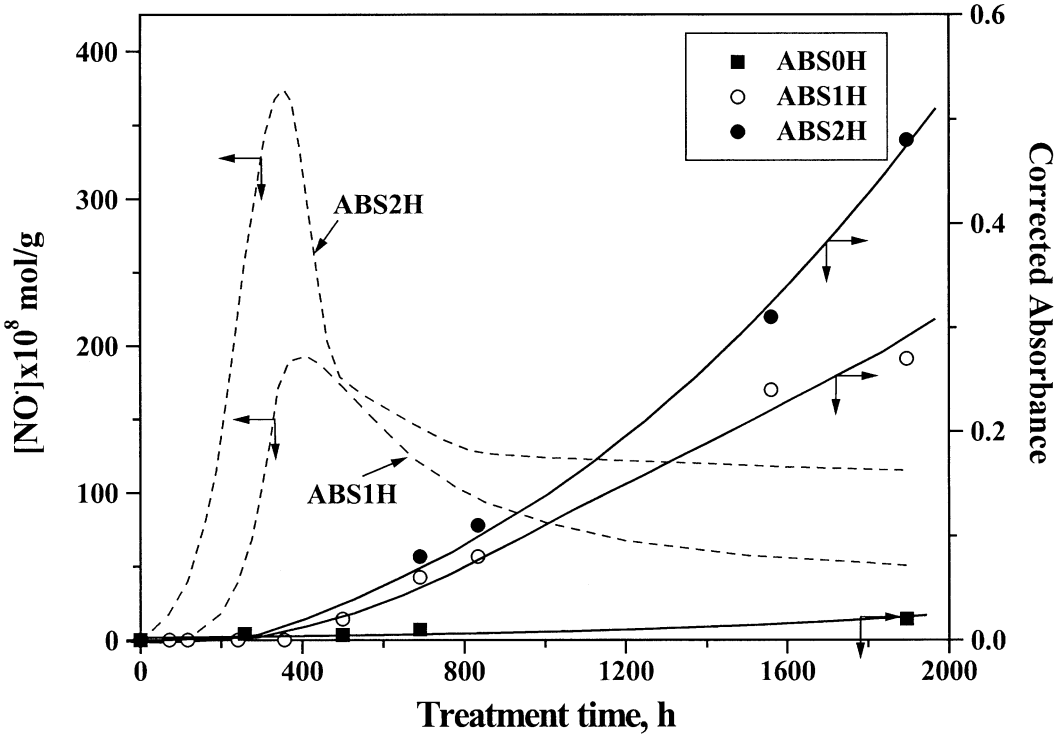

Fig. 9. Solid lines: the corrected absorbance in the carbonyl region (1731 cm^{-1}) as a function of treatment time at 393 K for ABS0H, ABS1H and ABS2H. The absorbance was obtained by subtracting the height of untreated samples from the corresponding heights of samples containing the same percentage of HAS. Dotted lines: the total nitroxide concentration (mol/g of sample) in ABS1H and ABS2H as a function of treatment time at 393 K. For clarity, the experimental points were omitted and only the lines drawn by nonlinear regression (Fig. 2B) are shown.

Changes in the carbonyl and butadiene regions, respectively, for ABS2H and ABS1H as a function of treatment time are given in Fig. 8B and C. In the carbonyl region the peak for the sample that was not treated (0 h in Fig. 8B) is assigned to the HAS. The increase of the carbonyl peak is observed only after ≈500 h of thermal treatment, but the increase is smaller in ABS1H than in ABS2H. Similarly, the decrease of the butadiene peak at 966 cm^{-1} (Fig. 8C) as a function of treatment time is more pronounced for ABS2H than for ABS1H.

The absorbance of the carbonyl (1731 cm^{-1}), and butadiene (966 cm^{-1}) peaks, respectively, as a function of treatment time is presented for ABS0H, ABS1H, and ABS2H in Figs. 9 and 10. For comparing ESRI and ATR–FTIR results, we also reproduce in Fig. 9 the variation of the total nitroxide concentration (from Fig. 2B), and in Fig. 10 the %F (from Fig. 2A), as a function of treatment time.

4. Discussion

In this section we will: discuss the importance of HAS content on ABS ageing; rationalize the destabilizing effect of HAS; and emphasize the advantage of the ESRI method in the early stages of degradation.

4.1. Effect of HAS content on ABS ageing

Hindered amines react with peroxy radicals and produce nitroxide radicals, which scavenge polymer radicals and form aminoethers (Fig. 1) [19]. Nitroxide formation requires the presence of oxygen. Therefore, for an understanding of the nitroxide profiles as a function of treatment time, it is instructive to consider the time dependence of the oxygen profile through the sample, which is often described as in Eq. (1) [2],

$$\frac{\partial[O_2]}{\partial t} = D\frac{\partial^2[O_2]}{\partial x^2} - f[O_2] \quad (1)$$

where D is the diffusion coefficient of oxygen, and $f[O_2]$ is a function that describes the oxygen consumption during polymer ageing. For low oxidation rates, for instance for the early stages of polymer ageing when the concentrations of reactive intermediates is low, $f[O_2]$ can be considered independent of oxygen content (zero-order kinetics regime), and a flat oxygen profile is expected.

For DLO conditions, however, $f[O_2]$ becomes dependent on oxygen concentration; if, for simplicity, first order kinetics is assumed, we obtain $f[O_2] = k_c[O_2]$, where k_c is the rate constant for oxygen consumption during polymer ageing. At steady state conditions, when the rate of

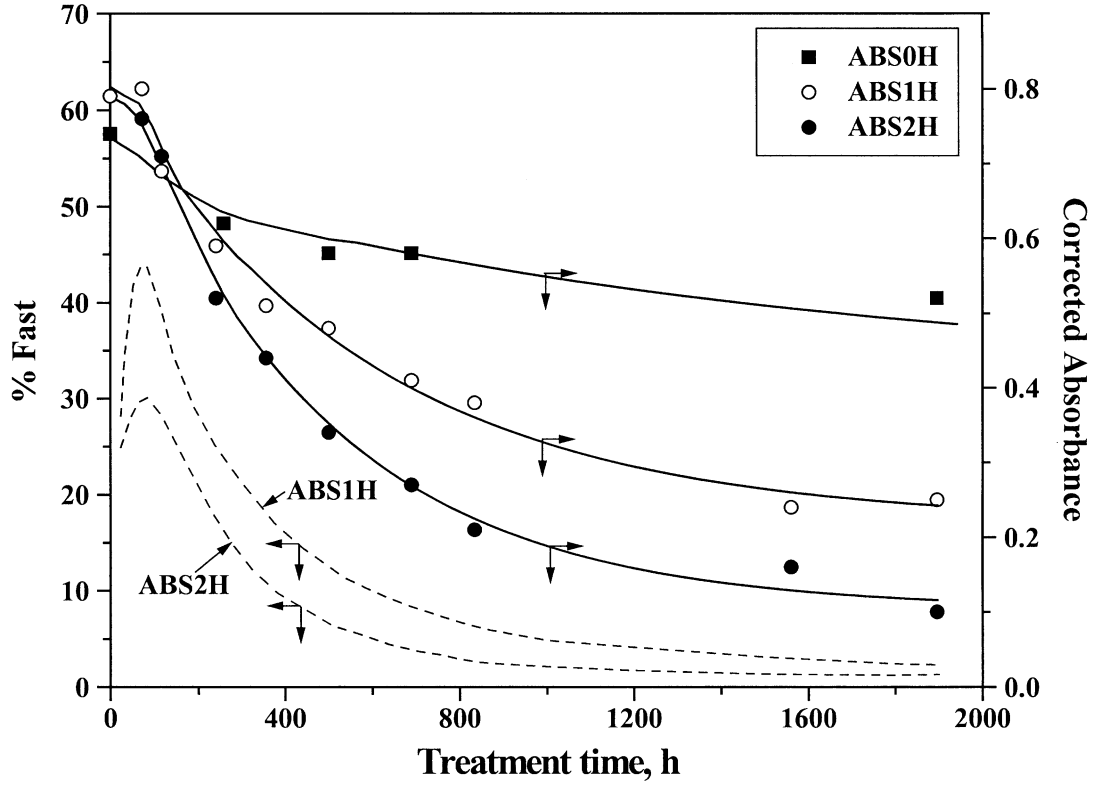

Fig. 10. Solid lines: the corrected absorbance in the 1,4-butadiene region (966 cm^{-1}) as a function of treatment time at 393 K for ABS0H, ABS1H and ABS2H. The absorbance from the corrected spectra was plotted. Dotted lines: the relative concentration of the fast component, %F, in ABS1H and ABS2H as a function of treatment time at 393 K. For clarity, the experimental points were omitted and only the lines drawn by nonlinear regression (Fig. 2A) are shown.

oxygen consumption is equal to the rate of oxygen supply by diffusion, the *degradation depth*, a, can be estimated from Eq. (1) [2,32], and defines the sample region where oxidation occurs. The degradation depth defined in Eq. (2) establishes the spatial range for the availability of oxygen, which is necessary for the formation of nitroxide radicals.

$$a \propto \sqrt{\frac{D}{k_c}} \tag{2}$$

Although a is not expected to be identical with the nitroxide depth, the concept is helpful in assessing the effect of the oxygen diffusion rate on the nitroxide distribution through the sample depth. More complicated kinetics schemes have been solved [2], but Eqs. (1) and (2) are helpful for qualitative comparison and interpretation of the 1D profiles shown in Figs. 3 and 4.

The zero-order regime is clearly seen in Fig. 4 for ABS2H, for treatment times of 24 h and (approximately) 72 h; similar profiles were obtained for ABS1H. For treatment times $t \geqslant 117$ h the change in the 1D profiles is indicative of the change in kinetics and the onset of DLO.

If we make the reasonable assumption that k_c in Eq. (2) is the same for ABS1H and ABS2H, the degradation depth in the DLO regime is expected to depend only on the oxygen diffusion coefficient, D. Indeed, in the case of styrene–butadiene rubber thermally aged at 423 K, a clear connection was established between the progressive spatial heterogeneity as measured by modulus profiling, and the decrease of the oxygen diffusion coefficient [33]. For the same D value, the degradation depth is expected to be lower for more advanced degradation.

The profile widths of the total nitroxide concentration for $t > 356$ h are larger for ABS1H compared to ABS2H, 700–800 μm vs 500–600 μm. We note that the spatial resolution of the ESR imaging experiments is better than ≈200 μm. The spectral profiles presented in Fig. 7 show similar results for the fast component, which is detected in a wider part of the sample in ABS1H compared to ABS2H, ≈650 μm vs 500 μm after treatment time of 834 h. Taken together the conclusions deduced from 1D and 2D ESRI are that the nitroxide radicals as well as the radicals in the butadiene-rich domains are located in a narrow layer of the sample, and this layer is wider in ABS1H compared to ABS2H. These results lead to the surprising conclusion that after relatively long treatment times, >400 h, the degradation is more advanced if the polymer contains more HAS.

The ATR–FTIR data presented in Figs. 8–10 provide additional support for the above conclusions: The

intensity of the carbonyl peak at a given treatment time is higher, and the intensity of the butadiene peak is lower, for ABS2H than for ABS1H. The ESRI and IR data are in agreement, and show the destabilizing effect of HAS *in the advanced stage of ageing*. The conclusion from the spectroscopic data are in agreement with the visual appearance of the samples: for the same treatment time, considerable more discoloration and shape distortion were seen in ABS2H, compared to ABS1H.

It is interesting to speculate on the widths of the nitroxide profiles in the *early* stages of ageing, $t < 356$ h. For $t = 117$ h, the profile for ABS2H is indicative of more homogeneous oxidation compared to ABS1H; this result might indicate better stabilization *in the initial phase* of the process when the amount of HAS is larger, possibly due to the removal of peroxides by HAS. The treatment time of 356 h seems to point to a change in the stabilization process, as for this treatment time the profiles for both samples have the same width. More work is needed in order to verify this idea.

4.2. The destabilizing effect of Tinuvin 770 in advanced ageing

The higher degradation rate in ABS samples containing more HAS can be explained by considering the reactions included in Fig. 1.

Nitroxide radicals combine with polymer radicals P$^\bullet$ to form aminoethers, $>$NOP, and can be regenerated by the reverse reaction $>\mathrm{NOP} \rightarrow > \mathrm{NO}^\bullet + \mathrm{P}^\bullet$. The products, $>$NO and P$^\bullet$, can also disproportionate to NOH and an olefin. Numerous studies have demonstrated the formation of $>$NO$^\bullet$ and P$^\bullet$ by thermal decomposition of aminoethers above ambient temperature, even below 373 K [34,35]. The rate of thermal decomposition of $>$NOP is higher in the presence of oxygen, which can scavenge the P$^\bullet$ radicals and form peroxides, POO$^\bullet$. Therefore, the process is more likely to occur on the surface layers in contact with air. In the case of polypropylene, the aminoether $>$NOP expected to form during photo-oxidation does not seem to regenerate $>$NO$^\bullet$, but the process is activated by thermal treatment [34]. The thermal sensitivity of the aminoethers might therefore be one reason for the lack of thermal stabilization by hindered amines.

In addition, nitroxide radicals at elevated temperatures are known to be powerful abstractors of hydrogen [34]. Polymer-derived radicals can be produced by the hydrogen abstraction reaction, $>\mathrm{NO}^\bullet + \mathrm{PH} \rightarrow > \mathrm{NOH} + \mathrm{P}^\bullet$. While NOH is known to deactivate POO$^\bullet$ radicals and is considered part of the nitroxide regeneration mechanism, the formation of P$^\bullet$ by hydrogen abstraction may be an additional important contribution to further ageing.

The reduced stabilization of monomeric HAS during thermal ageing of polypropylene has been explained by amine loss due to its volatility. The enhanced thermal antioxidant activity for a polymer-bound HAS compared to Tinuvin 770 was taken as a proof for this approach [19]. This idea, however, cannot explain the behaviour we detected in ABS, where the larger amount of HAS led to less stabilization.

It is important to note that in many applications, polymeric materials containing HAS are melt-processed at high temperatures, and under these conditions thermal degradation due to the presence of the amine can be a significant factor.

4.3. ESRI as a tool for the study of early events in polymer degradation

In Fig. 9 we presented the nitroxide concentration, [NO$^\bullet$], in ABS1H and ABS2H together with the corrected absorbance in the carbonyl region (1731 cm^{-1}), both as a function of treatment time. Similarly, in Fig. 10 both the %F in whole samples and the absorbance for the butadiene peak (966 cm^{-1}) are shown as a function of treatment time. The presence of the degradation product (carbonyl groups) and the decrease of the butadiene peak can be detected by IR spectroscopy in the advanced stages of ageing. The ESRI data are capable of providing details on ageing in the early stages of the process. For instance, the evolution from the flat profile (zero-order regime) to the DLO regime after a specific treatment time is visible by both 1D and 2D ESRI: in 1D ESRI from the total nitroxide profile, and in 2D ESRI from the nitroxide component present in the butadiene-rich domains, %F.

The ability to perform nitroxide profiling via 1D and 2D spectral–spatial ESRI in a polymer with a phase-separated morphology extends the spatial capability of the technique beyond the typical resolution achieved in magnetic resonance imaging. The result is the ability to visualize the variation of the HAS-derived nitroxide concentration due to degradation processes in morphologically-distinct domains in ABS within the sample depth with a resolution better than 200 μm.

5. Conclusions

Electron spin resonance imaging (ESRI) was applied to the study of thermal degradation at 393 K of poly(-acrylonitrile-butadiene-styrene) (ABS) containing 1 and 2% w/w Tinuvin 770 as the hindered amine stabilizer (HAS).

The spatial distribution of the radical intensity obtained by 1D ESRI was heterogeneous at 393 K after treatment times $\geqslant 70$ h. The spatial variation of the ESR spectra with sample depth was visualized by 2D spectral–spatial ESRI, and used to deduce the relative intensity of the nitroxide radicals in the two distinct sites along the sample depth. 1D and 2D ESRI allowed the determination

of the extent of degradation and stabilization in morphologically-distinct domains as a function of sample depth with a resolution better than 0.2 mm.

The conclusions from ESRI were supported by FTIR–ATR spectroscopy of the outer layer (500 μm thick) of the polymer. Both ESRI and FTIR data indicated that larger Tinuvin 770 content in the polymer (2%) leads to higher degradation rates.

Comparison of ESRI and IR methods emphasizes the advantage of the ESRI method: its sensitivity to early events in the ageing process.

Acknowledgements

This study was supported by the Polymers Program of NSF, and by a University Research Grant from The Ford Motor Company. S.S. is grateful for a Fellowship from the Institute of Advanced Study, University of Bologna in support of her 2001 sabbatical stay. It is a pleasure to thank Gian Franco Pedulli and Marco Lucarini for interesting discussions and for their hospitality in Bologna, Italy, where parts of this work were written. Special thanks are extended to Antonio Faucitano of the University of Pavia, Italy for discussions and ideas on nitroxide reactivity at elevated temperatures.

References

[1] Gillen KT, Clough RL. Rigorous experimental confirmation of a theoretical model for diffusion-limited oxidation. Polymer 1992; 33:4359.
[2] Billingham NC. The physical chemistry of polymer oxidation and stabilisation. In: Scott G, editor. Atmospheric oxidation and antioxidants, vol. II. Amsterdam: Elsevier; 1993. p. 219 (Chapter 4).
[3] Gillen KT, Clough RL, Dhooge NJ. Density profiling of polymers. Polymer 1986;27:225.
[4] Gillen KT, Clough RL, Quintana CA. Modulus profiling of polymers. Polym Degrad Stab 1987;17:31.
[5] Clough RG, Billingham NC, Gillen KT, editors. Polymer durability: degradation, stabilisation and lifetime prediction, Adv Chem Series 249. Washington (DC): American Chemical Society; 1996. p. 557 (Chapter 34).
[6] Gillen KT, Clough RL. Techniques for monitoring heterogeneous oxidation of polymers. In: Cheremisinoff NP, editor. Handbook of polymer science and technology. New York: M. Dekker; 1989. p. 167.
[7] Xavier J, Gardette JL. Photooxidation of ABS at long wavelengths. J Polym Sci A Polym Chem 1991;29:685.
[8] Hoekstra HD, Spoormaker JL, Breen J, Andouin L, Verdu J. UV-exposure of stabilised and non-stabilised HDPE films: physico-chemical characterisation. Polym Degrad Stab 1995;49:251.
[9] Celina M, George GA, Lacey DJ, Billingham NC. Chemiluminescence imaging of the oxidation of propylene. Polym Degrad Stab 1995;47:311.
[10] Matisova-Rychla L, Rychly J. New approach to understanding chemiluminescence from the decomposition of peroxidic structures in polypropylene. Polym Degrad Stab 2000;67:515.
[11] Blakey I, George GA. Simultaneous FTIR emission spectroscopy and chemiluminescence of oxidizing polypropylene: evidence for alternate chemiluminescence mechanisms. Macromolecules 2001; 34:1873.
[12] Schlick S, Pilar J, Kweon S-C, Vacik J, Gao Z, Labsky J. Measurements of diffusion processes in HEMA–DEGMA hydrogels by ESR imaging. Macromolecules 1995;28:5780.
[13] Malka K, Schlick S. Hydration, dynamics, and transport across the phase diagram of aqueous EO13PO30EO13 (Pluronic L64) by spin probe ESR and ESR imaging. Macromolecules 1997;30:456.
[14] Schlick S, Eagle P, Kruczala K, Pilar J. In: Blümler P, Blümich B, Botto R, Fukushima E, editors. Spatially resolved magnetic resonance: methods, materials, medicine, biology, rheology, ecology, hardware. Weinheim: Wiley-VCH; 1998. p. 221.
[15] Degtyarev EN, Schlick S. Diffusion coefficients of small molecules in various phases of Pluronic L64 measured by one-dimensional electron spin resonance imaging (1D ESRI). Langmuir 1999;15:5040.
[16] Motyakin MV, Gerlock JL, Schlick S. (a) Electron spin resonance imaging (ESRI) of degradation and stabilisation processes: behavior of a hindered amine stabiliser in UV-exposed poly(acrylonitrile-butadiene-styrene) (ABS). Macromolecules 1999;32:5463. (b) Electron spin resonance imaging (ESRI) of degradation and stabilisation processes in polymers. In: Mallinson LG, editor. Ageing studies and lifetime extension of materials. Kluwer: New York; 2001. p. 353.
[17] Kruczala K, Motyakin MV, Schlick S. 1D and 2D spatial–spectral electron spin resonance imaging (ESRI) of degradation and stabilisation processes in poly(acrylonitrile-butadiene-styrene) (ABS). J Phys Chem B 2000;104:3387.
[18] Motyakin MV, Schlick S. Spectral profiling by 1D and 2D electron spin resonance imaging: nitroxide radicals in UV and thermal degradation of poly(acrylonitrile-butadiene-styrene) containing a hindered amine stabiliser. Macromolecules 2001;34:2854.
[19] Scott G. Macromolecular and polymer-bound antioxidants. In: Scott G, editor. Atmospheric oxidation and antioxidants, vol. II. Amsterdam: Elsevier; 1993. p. 279 (Chapter 5).
[20] Schlick S, Motyakin MV. Behaviour of HAS-derived nitroxides in thermally degraded poly(acrylonitrile-butadiene-styrene) (ABS) based on ESR imaging and FTIR. Polym Prepr (Am Chem Soc Div Polym Chem) 2001;42(2):195.
[21] Lucarini M, Pedulli GF. Use of EPR to image nitroxyl radicals in HALS stabilized polymers. Angew Makromol Chem 1997;252: 179 [and references therein].
[22] Franchi P, Lucarini M, Pedulli GF, Bonora M, Vitali M. Time evolution of the concentration profiles of HALS stabilizers and of the corresponding oxidation forms across polypropylene plaques irradiated with UV-visible light. Macromol Chem Phys 2001;202:1246.
[23] Smirnov AI, Belford RL, Morse R. Magnetic resonance imaging in a hands-on student experiment using an EPR spectrometer. Concepts Magn Reson 1999;11:277.
[24] Motyakin MV, Schlick S, submitted for publication.
[25] Maltempo MM, Eaton SS, Eaton GR. In: Eaton SS, Eaton GR, Ohno K, editors. EPR imaging and in vivo EPR. Boca Raton (FL): CRC Press; 1991. p. 145 (Chapter 14).
[26] Marek A. 2000. Unpublished work from this laboratory.
[27] Celina M, Wise J, Ottesen DK, Gillen KT, Clough RL. Oxidation profiles of thermally aged nitrile rubber. Polym Degrad Stab 1998;60:493.
[28] Daniels ES, Dimonie VL, El-Aasser MS, Vanderhoff JW. Preparation of ABS latexes using hydroperoxide redox initiators. J Appl Polym Sci 1990;41:2463.
[29] Kulich DM, Gaggar SK. In: Clough RG, Billingham NC, Gillen KT, editors. Polymer durability: degradation, stabilisation and lifetime prediction, Adv Chem Series 249. Washington (DC): American Chemical Society; 1996. p. 483 (Chapter 31).
[30] Carter III. RO, McCallum JB. Photoacustic infrared spectroscopy of an ABS as an automotive interior material. Polym Degrad Stab 1994;45:1.

[31] Gerlock JL, Bauer DR, Briggs LM. Photo-stabilisation and photo-degradation in organic coating containing a hindered amine light stabiliser. Part I—ESR measurements of nitroxide concentration. Polym Degrad Stab 1986;14:53.
[32] De Bruin JCM. In: Clough RG, Billingham NC, Gillen KT, editors. Polymer durability: degradation, stabilisation and lifetime prediction, Adv Chem Series 249. Washington (DC): American Chemical Society; 1996. p. 599 (Chapter 36).
[33] Clough RL, Gillen KT. Oxygen diffusion effects in thermally aged elastomers. Polym Degrad Stab 1992;38:47.
[34] Pospisil J. Aromatic and heterocyclic amines in polymer stabilisation. Adv Polym Sci 1995;124:87.
[35] Rozantsev EG, Kagan ES, Sholle VD, Ivanov VB, Smirnov VA. Discovery, chemistry, and application of hindered amines. In: Klemchuk PP, editor. Polymer stabilisation and degradation, Symp Series 280. Washington (DC): American Chemical Society; 1985. p. 11 (Chapter 2).